Applied Energy 237 (2019) 566–580

Contents lists available at ScienceDirect

Applied Energy

journal homepage: www.elsevier.com/locate/apenergy

Thermohaline stratification modeling in mine water via double-diffusive convection for geothermal energy recovery from flooded mines

Ting Bao[a], Zhen (Leo) Liu[b,*]

[a] Department of Civil and Environmental Engineering, Michigan Technological University, 1400 Townsend Drive, Dow 854, Houghton, MI 49931, United States
[b] Department of Civil and Environmental Engineering, Michigan Technological University, 1400 Townsend Drive, Dillman 201F, Houghton, MI 49931, United States

HIGHLIGHTS

- Address a key scientific question for geothermal application with mine water.
- Reproduce the layering phenomenon in mine water for the first time.
- Obtain a numerical framework for design and analysis of the energy innovation.
- Identify layer-merging events and factors such as critical buoyancy ratios.

ARTICLE INFO

Keywords:
Double-diffusive convection
Mine water
Geothermal energy
Buoyancy ratio
Thermohaline stratification

ABSTRACT

This study addresses a key scientific issue that remains unresolved in the past three decades for recovering geothermal energy from flooded mines. This issue is that no scientific explanation is available for the layering phenomenon of both temperature and salinity in large bodies of subterranean water (e.g., mine water), i.e., thermohaline stratification, which is commonly observed in mine water. Such a layering phenomenon, however, is very significant to the geothermal application by determining the temperature distribution and consequently the energy reserve and efficiency. For this purpose, multiphysics simulation with unique non-isothermal and non-isosolutal hydrodynamics is adopted to predict the formation and evolution of thermohaline stratifications in large bodies of mine water. The multiphysics simulation, for the first time, succeeded in reproducing the formation and evolution of thermohaline stratifications with a theory assuming lateral double-diffusive intrusions to mine water. The simulation results revealed that the evolution of thermohaline stratifications involves the layer-merging event, in which several small layers gradually merge to form layers with a larger thickness. The results also indicated that the buoyancy ratio is a key parameter for producing clear thermohaline stratifications in large bodies of mine water and its critical value was suggested to be 1.0. To successfully reproduce thermohaline stratifications, the required condition was concluded to be the lateral heat flux with a difference between the lateral heat fluxes, while the lateral salinity flux was not required. It is the first time, to the best of our knowledge, that the layering phenomenon in large-scale subterranean water bodies has been successfully reproduced and explained scientifically. This study will provide a solid scientific basis for the efficient and sustainable use of large bodies of subterranean water in flooded mines for geothermal energy recovery.

1. Introduction

As an alternative energy source, geothermal energy provides green [1], sustainable [2], eco-friendly and renewable energy [3] for humanity's energy demands. Geothermal energy can be used for electric power generation due to its advantages, such as environment-friendliness and cost-competitiveness over conventional sources of energy [4]. Exploring geothermal energy for electric power generation needs specific qualifications, e.g., a very high enthalpy fluid or vapor; as a result, only specific locations in about 24 countries could generate electricity with geothermal resources [5]. Another direct use of geothermal energy is to heat or cool buildings using geothermal heat pumps in the U.S. [6] and around the world [7]. Such pumps can transfer heat from materials (e.g., water and soils) with the low enthalpy to a high enthalpy fluid via the circulation of a working fluid in heat pumps [8], which thus can enable heating/cooling of buildings

* Corresponding author.
E-mail addresses: tbao@mtu.edu (T. Bao), zhenl@mtu.edu (Z.L. Liu).

https://doi.org/10.1016/j.apenergy.2019.01.049
Received 24 May 2018; Received in revised form 17 December 2018; Accepted 4 January 2019
Available online 11 January 2019

Nomenclature

h_{rf}	rock-flow heat transfer coefficient [W/m^2/K]
h_f^T	flow-flow heat transfer coefficient [W/m^2/K]
h_f^S	salt transfer coefficient [m/s/%]
$\mathbf{g}$	gravitational acceleration vector [m/s^2]
G	heat or salt gradient [K/m or %/m]
F_r	rock heat flux [W/m^2]
F_f^T	flow heat flux [W/m^2]
F_f^S	flow salt flux [m/s]
ΔF_f^T	flow heat flux difference [W/m^2]
ΔF_f^S	flow salt flux difference [m/s]
t	time [s]
p	total pressure [Pa]
p_d	hydrodynamic pressure [Pa]
T_0	reference temperature [K]
T	temperature [K]
T_t	top temperature [K]
T_b	bottom temperature [K]
T_d	temperature difference [K]
$\mathbf{U}$	velocity [m/s]
S_0	reference salinity [%, w/w]
S	salinity [%, w/w]
S_t	top salinity [%, w/w]
S_b	bottom salinity [%, w/w]
R	represents T_t or S_b [K or %]
z	elevation [m]

Dimensionless numbers

N	buoyancy ratio
N_c	critical buoyancy ratio
Le	Lewis number
Pr	Prandtl number
Ra	Rayleigh number
Sc	Schmidt number

Greek symbols

ρ	density [kg/m^3]
ρ_0	reference density [kg/m^3]
ν_{eff}	effective kinematic viscosity [m^2/s]
β_T	thermal expansion coefficient [K^{-1}]
β_S	solutal expansion coefficient [%$^{-1}$]
α_T	thermal eddy diffusivity [m^2/s]
α_{eff}^T	effective thermal diffusivity [m^2/s]
α_{eff}^S	effective solutal diffusivity [m^2/s]

with energy from the low enthalpy (temperature) source. Conventional applications of geothermal heat pumps involve the heat exchange between working fluids in pipes and the surrounding ground (e.g., borehole) in ground-coupled heat pump applications or the heat exchange between working fluids in pipes and water in wells in ground-water heat pump applications. To obtain a higher energy efficiency, such direct use of geothermal energy requires drilling to access deep locations that have a greater temperature difference with the working fluids. This may raise economic and technical concerns in some areas because of the significant investments in geothermal borehole/well constructions and uncertainties in borehole/well drilling.

Underground mining exists in almost every country. A great number of underground mines in numerous counties were closed and abandoned in the past decades, and many of them were flooded with water, either naturally or artificially, after their closure [9]. Flooded mines are usually hundreds or even thousands of meters deep in the ground. The water in the mines, i.e., mine water, can reach the lower portions of shafts and drifts with high temperatures and can be continuously heated by the Earth's geothermal energy, leading to a stable high temperature contrast with the air without additional drilling work. Due to this benefit, increasing research attention has been paid to the recovery of geothermal energy from flooded mines for geothermal applications since the pioneering work in Canada in 1989 [10]. Mine water with high temperatures can run through a heat exchanger for heating or/and cooling buildings. This novel concept offers more benefits than the conventional ground-coupled heat pump applications and ground-water heat pump applications. First, mine water offers much better heat transfer and a much higher energy reserve by greater orders because tens or hundreds of million cubic meters of mine water provides an enormous bulk and mobile medium for energy storage and transfer than that of soils and water in wells used in the conventional ones. Also, mine water is currently treated as a useless material and isolated from daily life, the use of mine water for geothermal applications is thus safe, green, relatively renewable, adaptable, and eco-friendly. Finally, as mentioned above, abandoned mines with mine water are existing facilities, therefore, no extra cost is needed for their construction, which saves a significant amount of expenditure compared to the conventional ones.

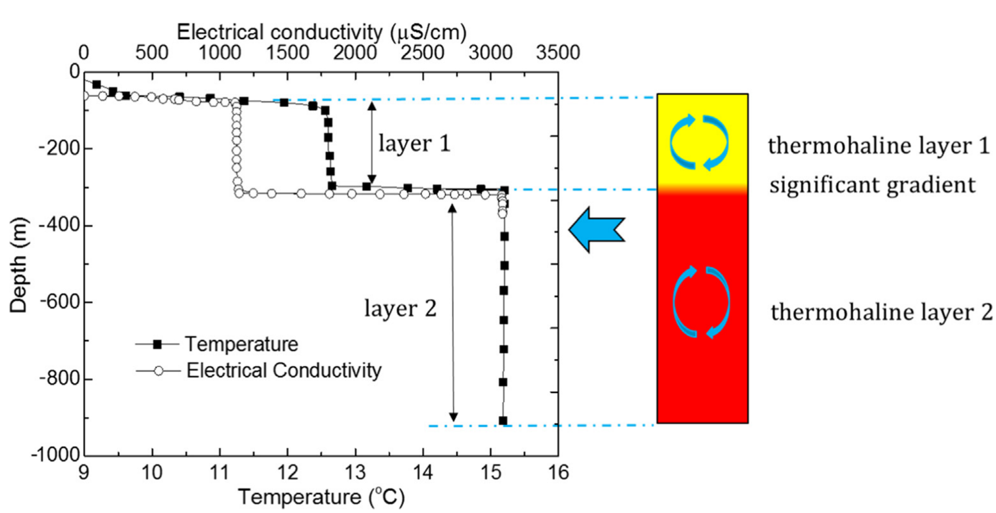

Fig. 1. Typical thermohaline stratifications from field measurements (modified after [29]).

Practical attempts have been made for exploring mine water as a renewable geothermal resource. A realistic utilization of a flooded mine as a large reservoir of heat was implemented in Canada [10]. This application proved that the extraction of energy from flooded mines beneath the community for heating/cooling buildings is not only feasible but also environment-friendly due to a stable high temperature contrast with the air provided by mine water and a reduction in carbon dioxide emissions [11]. Observations from later field measurements or evaluations of available geothermal data, such as in Poland [12], Netherlands [13], Germany [14], and Spain [15], also revealed that the water in closed mines contains a great reserve of geothermal energy. Additional efforts also have been made to investigate several essential aspects of the application: the thermal energy reserve and the later energy replenishment from the surroundings [14], typical investments and corresponding economic paybacks [16], effective and suitable geothermal energy recovery systems [17], effective velocities of mine water [18], and potential environmental impacts [19]. Currently, the performance of real applications has also been evaluated via measurements of temperatures in mine water. In the U.K., two real installations of tapping geothermal energy from a single shaft in Markham [20] and Wakefield [21] revealed that the mine water temperature did not vary during the long-term heat extraction period. These studies confirmed the high sustainability and reliability of heating buildings with mine water.

Despite the above progress in real installations, the scientific understanding of geothermal energy recovery from flooded mines is still far behind its implementations. Numerical studies have been carried out to understand the sustainability of the heat extraction from flooded mines, e.g., a period of 50 years for extracting heat [22] and the sustainable energy extraction rate [23], and the heat transport mechanisms underlying temperature variations in mine water for the application using a hydraulic model [24], a hydrogeological and thermal model [25], and a thermo-hydrodynamic model [26]. However, the dominant heat and mass transport mechanisms in large bodies of subterranean water, i.e., mine water spontaneously stratifies into layers with different temperatures and salinities [27], have not been explained in those published studies. As shown in Fig. 1, the layering phenomenon produced by such dominant mechanisms demonstrates that each layer has an approximately uniform temperature and salinity. Significant changes in the temperature and salinity occur at the interface between two adjacent layers. This observation indicates that mine water is possibly mobile and well-mixed in each individual layer. This layering phenomenon is termed the thermohaline stratification that may share similar evolution mechanisms for thermohaline staircases in oceans [28]. The thermohaline stratification could play a crucial role in the geothermal energy recovery. For extracting heat with mine water, an open-loop heat pump is widely used in practice, e.g., two installations in Markham [20] and Wakefield [21]. Since the thermohaline stratification governs the temperature distribution and variation in mine water, it determines the spatial distributions and temporal variations of the temperature in the water. The available water temperature directly determines the efficiency of the heat pumps and consequently that of the whole geothermal systems. The long-term variation of the water temperature determines whether the geothermal application is sustainable in a long run. More importantly, the decision-making on the pumping locations and pumping rates for the design and operation of the geothermal energy system will, in return, affect the energy and mass transport dominated by the thermohaline stratification. One possible scenario is that geothermal energy recovery using mine water can even possibly break the thermohaline stratification in some cases, which may bring forth either beneficial or adverse impacts on the energy application. However, all of these are just guesses due to the lack of a sound understanding of the natural mine water system. The major reason is that there has been no explanation for the layered water structure, which is the major heat and mass transport in mine water, let alone studies for the interaction of the geothermal system with the natural mine water system. Therefore, it is urgent and essential to obtain an understanding of the major heat and mass transport mechanisms in mine water. Based on that, we can design geosystems and predict their behavior.

Though not extensively, a very few numerical studies have been carried out to understand the heat and mass transport mechanisms in water mine for understanding thermohaline stratifications. Hamm and Sabet [30] modeled the hydraulic behavior of the mine reservoir and mine water temperature in a production shaft to reveal the influences of the natural thermal convection on the geothermal energy recovery. However, this model [30] simulated the natural thermal convection without considering salinity transport. Both heat and salinity transport processes need to be considered as mine water movement is driven by the buoyancy force that is determined by heat and salinity simultaneously. This coupled process for mine water movement is called the Double-Diffusive Convection (DDC). Heat and salinity transfer simultaneously in mine water with different diffusivities and more significantly affect the vertical density gradient of mine water in the opposite way [31]. Warm water is less dense than cold water, while salty water is more dense than fresh water. Reichart et al. [32] numerically investigated the DDC process in mine water with a focus on testing thermal and solutal convections using a 2-Dimensional (2D) model. However, the computational scale of mine water was too small (around 1 m) to reflect the real dimensions (around 1 km or greater) in natural water bodies and the thermohaline stratification was not successfully obtained. Therefore, the formation of thermohaline stratifications in large bodies of subterranean water is an unclear scientific issue that remains unresolved in the past three decades due to the complexity of the physical transport mechanisms.

In this study, we address this unresolved but key scientific issue using a fully coupled DDC numerical model. The main objective is to predict the formation and evolution of thermohaline stratifications in large bodies of subterranean water (around 1.2 km), which is of great significance for the utilization of mine water for geothermal applications. This study is organized as follows. A theoretical framework for the coupled model is described first and then validated against documented results. Then, two hypotheses for the formation of thermohaline stratifications in oceans are introduced and discussed. Afterward, multiphysics simulation with unique non-isothermal and non-isosolutal hydrodynamics is conducted using the validated model. Based on the simulation, the primary physical mechanisms are investigated and in-depth discussions are made to shed light on the formation and evolution of thermohaline stratifications in the large-scale mine water from a scientific perspective.

2. Theory and method

2.1. Mathematical formulation

This section outlines a theoretical framework for modeling the DDC process in mine water. Due to the temperature and salinity gradients, mine water moves naturally with double diffusion in the underground mining spaces. In this situation, mine water is assumed to be Newtonian and incompressible except for the gravity. The continuity equation for the mass conservation is formulated as

$$\nabla \cdot \mathbf{U} = 0 \tag{1}$$

where $\mathbf{U}$ is the velocity of mine water. The conservation of momentum for the fluid element is formulated using the following equation

$$\frac{\partial \mathbf{U}}{\partial t} + \mathbf{U} \cdot \nabla \mathbf{U} = -\frac{\nabla p_d}{\rho_0} + \nabla \cdot (\nu_{eff} \nabla \mathbf{U}) + \frac{\rho}{\rho_0}\mathbf{g} \tag{2}$$

where ν_{eff} is the effective kinematic viscosity of mine water, ρ is the density of mine water, ρ_0 is the reference density of mine water, $\mathbf{g}$ is the gravitational acceleration vector, and p_d is the hydrodynamic pressure and given by

$$p_d = p - \rho gz \tag{3}$$

where p is the total pressure, z is the elevation, and ρgz is the hydrostatic pressure. To consider the buoyancy force induced by temperature and salinity differences, the Oberbeck-Boussinesq approximation [32] is used, in which the density ρ varies linearly with the temperature T and solute concentration S of mine water:

$$\rho = \rho_0[1 - \beta_T(T - T_0) + \beta_S(S - S_0)] \tag{4}$$

where β_T is the coefficient of thermal expansion, β_S is the coefficient of solutal expansion, and T_0 and S_0 are the reference temperature and salinity, respectively.

The energy conservation of the moving fluid element is formulated as

$$\frac{\partial T}{\partial t} + \mathbf{U}\cdot\nabla T = \nabla\cdot(\alpha_{eff}^{T}\nabla T) \tag{5}$$

where α_{eff}^{T} is the effective thermal diffusivity of mine water. The transport of solutes within the moving fluid element is governed by

$$\frac{\partial S}{\partial t} + \mathbf{U}\cdot\nabla S = \nabla\cdot(\alpha_{eff}^{S}\nabla S) \tag{6}$$

where α_{eff}^{S} is the effective solutal diffusivity of mine water.

In the dynamic DDC system, both temperature and salinity determine the water movement via controlling the buoyancy force. To evaluate the relative influence of salinity and temperature on the buoyancy force, the buoyancy ratio is defined in the system using the following equation

$$N = \frac{\beta_S \Delta S}{\beta_T \Delta T} \tag{7}$$

where ΔS and ΔT are the salinity and temperature differences along the vertical axis of a shaft.

The governing equations presented above were discretized and solved using an open-source finite volume method platform, OpenFOAM, which utilizes different schemes for discretization. The time was discretized using the Euler scheme. The Gaussian linear integration was used for discretizing all the gradient and divergence terms. The discretization for the Laplacian terms was the Gaussian linear scheme with limited corrections. Details regarding the discretization of the governing equations can be found in Ferziger and Peric [33]. The PISO algorithm was used in this study to solve the

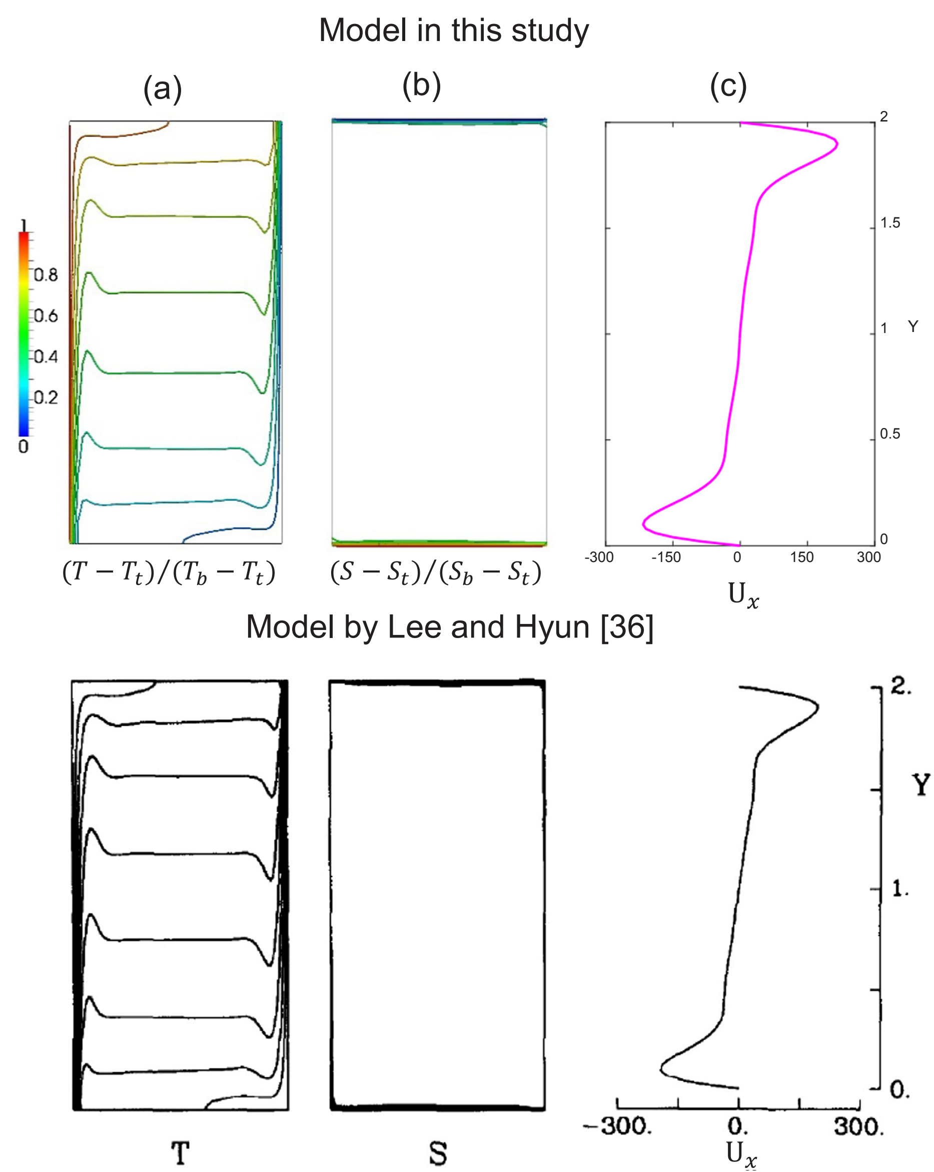

Fig. 2. Comparisons between the results from the model in the current study and the numerical results from Lee and Hyun [36]: (a) dimensionless temperature contour, (b) dimensionless salinity contour, and (c) dimensionless horizontal velocity vs dimensionless vertical axis.

iteration of the coupled system [34], which applies one predictor step and two corrector steps to obtain a desired accuracy of the pressure and velocity.

2.2. Numerical model validation

In this section, the theoretical framework developed in Section 2.1 is validated against documented numerical results. DDC was experimentally investigated [35] in a rectangular enclosure under a vertical salt gradient and a horizontal temperature gradient to reveal the temperature and salinity distributions within the enclosure when the steady state of DDC was reached. A numerical study [36] was conducted later to verify the observations from the experiment [35] by indirectly comparing the DDC flow pattern. The numerical study provided transient DDC results and was conducted in a rectangular enclosure with an aspect ratio of (vertical 0.04 m; horizontal 0.02 m) 2:1 under a vertical salt gradient and a horizontal temperature gradient. Different buoyancy ratios were investigated and transient simulation calculations were continued until the quasi-steady state was reached to approximate the steady DDC results of the experiment [35].

The simulation in this section is designated for model validation via comparisons against the numerical results [36]. The same dimensions as [36] were used. The adopted parameters for the simulation are as follows: the buoyancy ratio $N = 3$; the Rayleigh number $Ra = 10^7$; the Prandtl number $Pr = 7$; and the Lewis number $Le = 100$, i.e., the Schmidt number $Sc = 700$. For the initial condition, the initial temperature within the enclosure was uniform with T_t, while the initial salinity was linearly distributed from S_t (top wall) to S_b (bottom wall). For the boundary condition, the left wall and the right wall were set up with no solutal flux but with fixed temperatures of T_b and T_t, respectively; the top wall and the bottom wall were set up with the no thermal flux but with fixed salinities of S_t and S_b, respectively. The above initial and boundary values for the temperatures and salinities were calculated based on N and Ra strictly following Lee and Hyun [36]. 0.1 s was selected as the time step. The grid used for the simulation consisted of 50 and 100 identical cells in the horizontal and vertical directions, respectively. The grid resolution was 4×10^{-4} m.

Shown in Fig. 2 are the comparisons between the results computed by the model in this study and the published numerical results [36]. The dimensionless temperature contour, salinity contour, and the horizontal velocity distribution are in good agreement with the published numerical results [36]. Due to a small buoyancy ratio, i.e., $N = 3$, the thermal convection dominants the water movement in the whole enclosure. Therefore, the salinity in the interior enclosure is well mixed to be uniform by the thermal convection. The salinities on the top and bottom boundaries are fixed and different from the salinity in the interior enclosure. Due to this salinity difference, the iso-solutal lines are located in very small regions adjacent to the top and bottom walls. The good agreement in Fig. 2 indicates the good capacity and accuracy of the newly developed model in Section 2.1 for simulating the DDC process.

2.3. Hypotheses of thermohaline stratification

The layering phenomenon is commonly observed in oceans where temperature and salinity vary vertically in a step-like shape [37], which is thus called thermohaline staircases in oceans. This phenomenon is associated with dynamic DDC due to the existence of temperature and salinity simultaneously. Two types of DDC can occur if large-scale gradients of temperature and salinity exist in the vertical direction: (1) the salt-finger (warm and salty water overlies cold and fresh water) and (2) the diffusive convection (cold and fresh water overlies warm and salty water). As the salt-finger is more common and vigorous in the ocean [38], this type, therefore, has been investigated more extensively than the diffusive convection for understanding the formation of thermohaline staircases in oceanic regions.

To date, two hypotheses, which have been proven by numerical studies to some extent, are available to explain the formation of thermohaline staircases. Merryfield [37] proposed that thermohaline staircases arise from double-diffusive intrusions caused by lateral temperature and salinity gradients. Radko [39] recently proposed the second hypothesis that thermohaline staircases are caused by the gamma instability driven by variations in the ratio of the turbulent heat and salt fluxes. For thermohaline staircases modeling in oceans, the second hypothesis (i.e., the gamma) has succeeded in simulating thermohaline staircases in the large-scale oceanic water circulation with a water surface area of 1000 km^2 and a water depth of 1 km [28].

As for mine water, its dynamic DDC belongs to the diffusive convection due to the geothermal (temperature) and geochemical (salinity) gradients. Though less discussed in oceanography, the major cause of thermohaline staircases in the diffusive convection (i.e., second DDC type) is believed to be similar to that in the salt-finger (i.e., first DDC type) [28]. For thermohaline staircases of the salt-finger obtained with the second hypothesis [39], the key step is that the gamma is ensured to be a variable rather than a constant to successfully produce thermohaline staircases [28]. This gamma is primarily governed by temperature and salinity differences between the ocean surface and ocean bottom. As bottom temperature and salinity keep unchanged, the surface temperature and salinity are required to vary in order to obtain a variable gamma. A variable gamma is common in oceans because of the wide ocean surface influenced by solar irradiance. However, due to the narrow water surface area constrained by shaft configurations and the negligible influence of solar irradiance, the value of the gamma in mine water is very likely to be a constant. This implies that the second hypothesis could not be used to explain the formation of thermohaline stratifications in mine water. Therefore, we adopt the first hypothesis to predict the formation of thermohaline stratifications in the large bodies of mine water in the following. That is, the major cause for the layering phenomenon in mine water is hypothesized to be the double-diffusive intrusion induced by lateral temperature and salinity fluxes.

2.4. Model configuration for layering simulation

The Hancock mine located in the Upper Peninsula (U.P.) of Michigan was flooded with water after its closure due to the high level of the groundwater table. According to field observations in the U.P. from Hancock Shaft 2 [29], there are at least two layers in mine water and each layer has an approximately uniform temperature and salinity (indirectly measured by electrical conductivity) (see Fig. 1). Therefore, Hancock Shaft 2 was chosen for the simulation in the following subsection.

Fig. 3 shows the 2D model configuration and its grid developed based on the realistic underground mine layout of the Hancock mine according to Butler and Burbank [40]. The model was configured to have grids with a resolution of 0.4 m for the mine water body in the shaft and drifts, and with a very high resolution of 0.01 m for regions on boundaries. One reason for this configuration is that our trial calculations showed that the DDC flow structure depends on the resolution of grids, therefore, thermohaline stratifications could not be observed with a low resolution of grids (e.g., 1 m in the horizontal direction). Another reason is that such a high resolution of grids on boundaries is helpful for ensuring the numerical stability when we consider the double-diffusive intrusion due to lateral heat and salt fluxes.

The initial temperature and salinity within large bodies of mine water were assumed to be linearly distributed with the depth along the shaft axis. The temperature varies from 282.15 K to 288.35 K according to field measurements [29]. It is worthwhile to mention that the mine water temperatures in this mine are relatively low for heating buildings, though the economic benefits with such temperatures have been confirmed in a local demonstration project running since 2009 [41]. Higher water temperatures or a more balanced heating need, e.g., in a region with higher air temperatures, may enhance the economic benefits of the

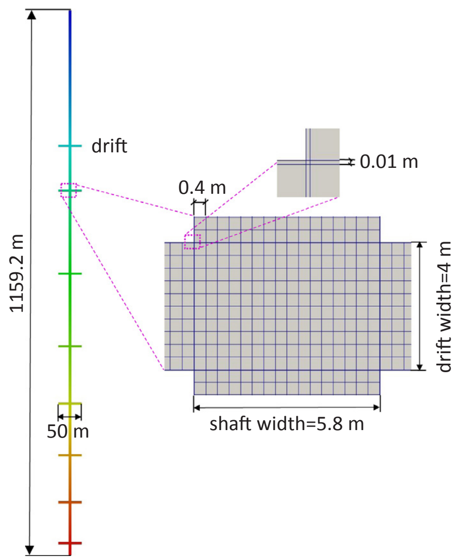

Fig. 3. 2D model configuration and grid.

Table 1
Parameters used in the DDC simulation.

Material	Parameter	Value
Mine water	Reference density (kg/m^3)	1088.6
	Reference temperature (K)	333.15
	Reference salinity (%)	15
	Specific heat (J/(kg K))	4181
	Effective viscosity (m^2/s)	3.95×10^{-3}
	Thermal expansion coefficient (K^{-1})	5.24×10^{-4}
	Solutal expansion coefficient (%$^{-1}$)	6.82×10^{-3}
	Effective thermal diffusivity (m^2/s)	4.94×10^{-4}
	Effective solutal diffusivity (m^2/s)	1×10^{-6}

Note: Thermal and solutal properties of mine water are determined from [44].

geothermal application with mine water significantly. For salinity in the Hancock mine, the top salinity S_t was assumed to be 0.01%, while the bottom salinity S_b was calculated with Eq. (7) based on the known buoyancy ratio N, S_t, and the temperature difference ΔT (i.e., 6.2 K). S_b at the bottom is 0.61% and 1.91% when N is equal to 1.26 and 4.0, respectively. Such two N values were estimated according to the local hydrologists and will be used in this study in Section 3.1.

The boundary conditions were implemented with the double-diffusive intrusion due to lateral temperature and salinity fluxes. The mass of mine water was assumed to be constant because the Hancock mine was flooded with groundwater soon after its closure and the current water level in the shaft reaches to its adit, leading to a stable water level. Therefore, only the lateral influx to mine water was considered. Fig. 4 shows the schematic of the boundary conditions for the simulation. In Fig. 4a, there is neither heat nor salt flux on the top surface or at the bottom. In the lateral directions, heat flux exists on both sides and will influence the temperature distribution of mine water. Heat flux values from rocks on the lateral boundaries (i.e., F_r in Fig. 4a) are identical due to the same geothermal gradient. In addition to the influx from rocks, the temperature of mine water can also be influenced by the heat flux (i.e., F_f^T) from the water flows through cracks and fissures in rocks. It is thus beneficial to consider the thermal coupling between mine water and these water flows through rocks. However, the consideration of

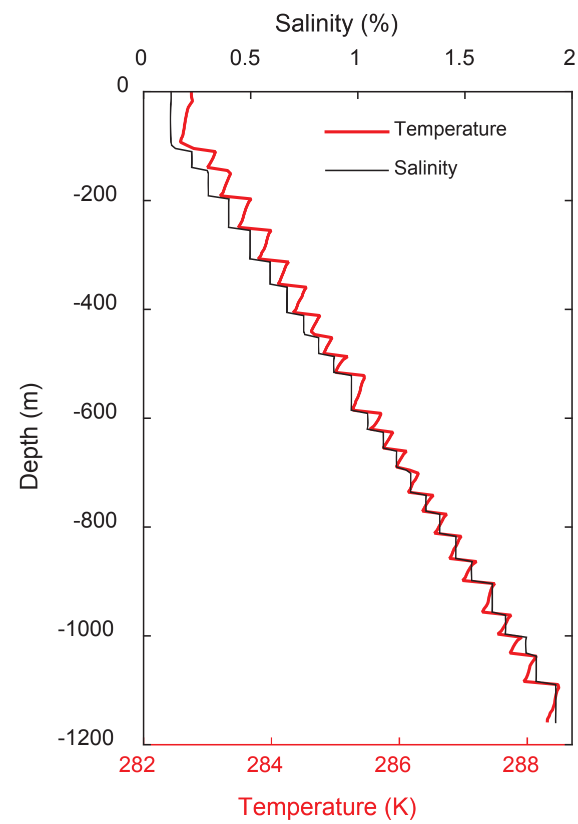

Fig. 5. Vertical distributions of temperature and salinity along the center axis of Shaft 2 when $N = 4$ at $t = 4.5$ days.

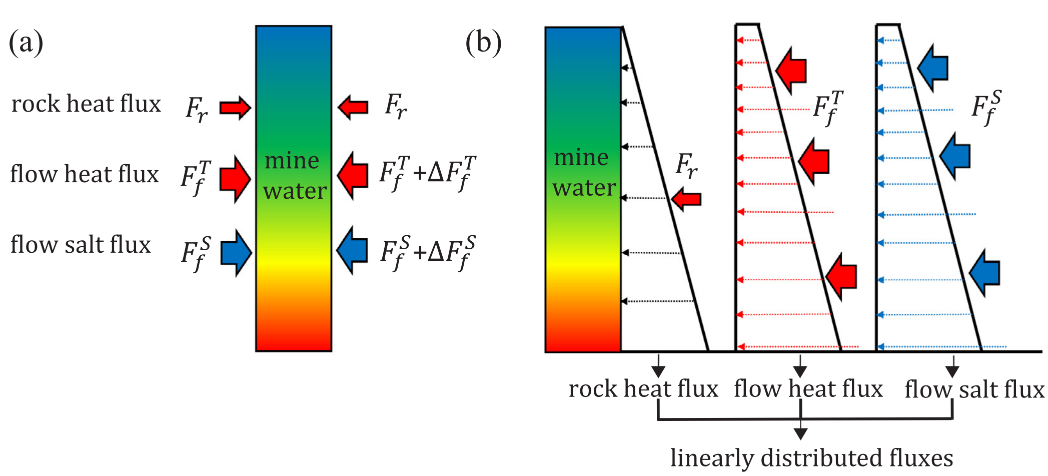

Fig. 4. Schematic of the boundary conditions of mine water body in the shaft with double-diffusive intrusions by lateral temperature and salinity fluxes: (a) the whole process of intrusions and (b) linear distribution of fluxes with depths.

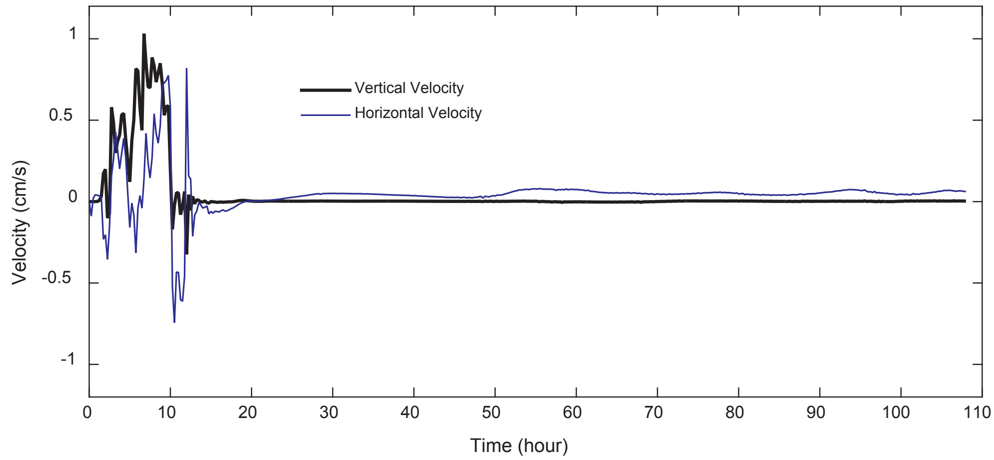

Fig. 6. Variations of mine water velocity with time when $N = 4$ in the center axis of Shaft 2 at the location $z = -470$ m.

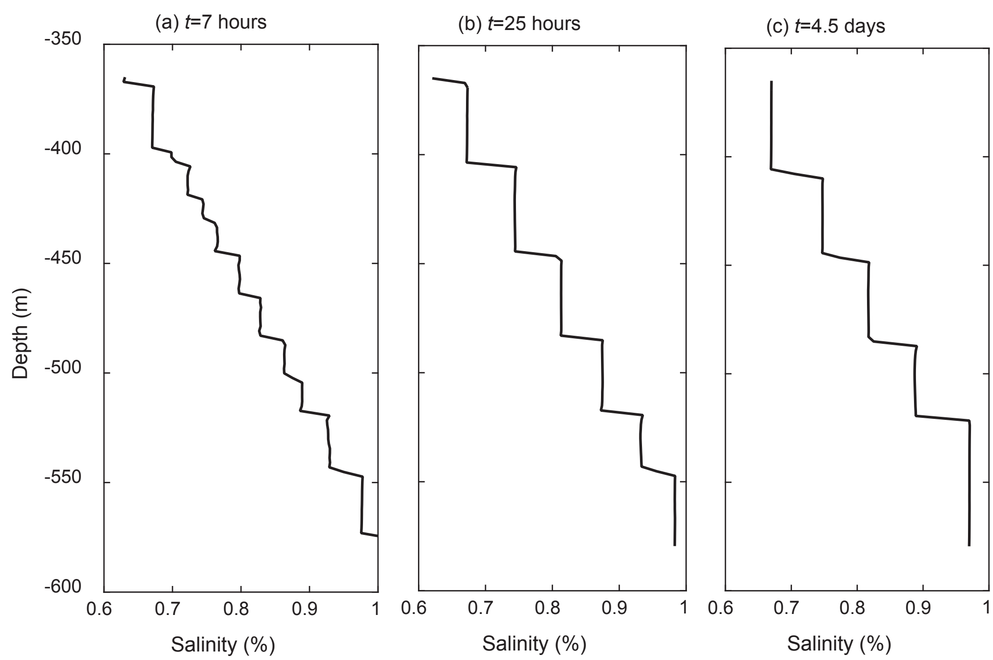

Fig. 7. Formation and evolution of stratifications for salinity when $N = 4$ in the elevation region between $z = -360$ m and $z = -579.6$ m: (a) $t = 7$ h, (b) $t = 25$ h, and (c) $t = 4.5$ days.

such a thermal coupling is very difficult. The first difficulty is that heat convection exists at the interface between mine water and the water flows through rocks. To solve this, heat convection between them was not considered directly and we assumed that only heat conduction exists at their interface. Instead, heat convection will be indirectly considered using a high value of the heat transfer coefficient between mine water and these water flows through rocks. The second difficulty is that the locations, where the water flows enter the shaft through any cracks, fissures, and faults in rocks, are unpredictable due to the complexity of the underground mine configurations. To resolve this difficulty, as shown in Fig. 4b, a linear distribution of the heat flux with the depth on the lateral boundaries was assumed. This assumption can cover all possible locations for the water flows to enter the shaft through cracks, fissures, and faults in rocks.

The influx to the mine water is also directly related to the overall groundwater movement through this shaft. The groundwater from the Jacobsville sandstone aquifer will flow in the direction toward the Keweenaw fault and toward the greatest depth [42], which is located toward the top of the U.P. of Michigan. This can give the groundwater a northeastern movement through the shaft, leading to the heat flux to the mine water during this overall groundwater movement. To consider this influx, we assumed that there is a difference between the lateral heat fluxes (i.e., ΔF_f^T).

As for the salt flux (i.e., F_f^S), the initial salinity of mine water can be influenced by the water flows through rocks only. Similar to the heat flux, we assumed that the distribution of the salt flux is linear with the depth and there is a difference between the lateral salt fluxes (i.e., ΔF_f^S). Due to the same geothermal (temperature) and geochemical (salinity) gradients for the water flows through rocks, ΔF_f^T and ΔF_f^S in Fig. 4(a) can be obtained when the top (i.e., $z = 0$) temperature and salinity of the water flows through rocks to the two lateral boundaries are different. Mathematically, the above assumptions linked to the double-diffusive intrusion due to lateral fluxes in Fig. 4 are described using the following formulations

$$\begin{cases} F_r = h_{rf}(r^T(z) - T) \\ F_f^T = h_f^T(r^T(z) - T) \\ F_f^S = h_f^S(r^S(z) - S) \\ \quad r(z) = R + zG \end{cases} \tag{8}$$

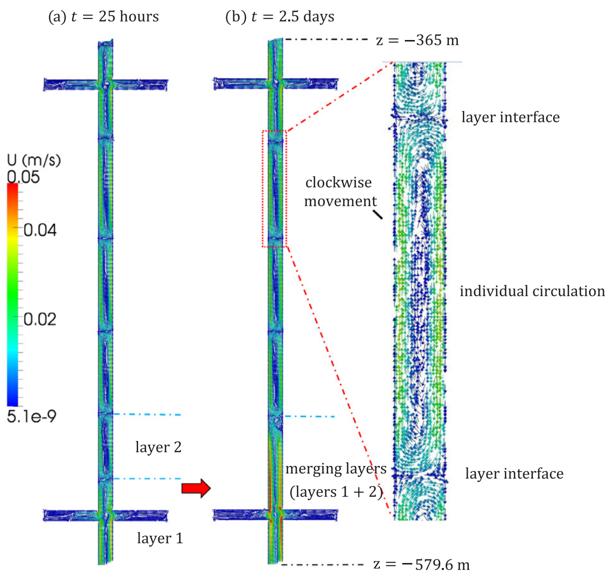

Fig. 8. Flow patterns of mine water in the region between $z = -365$ m and $z = -579.5$ m: (a) $t = 25$ h and (b) $t = 2.5$ days.

where h_{rf} is the heat transfer coefficient between mine water and rocks, h_f^T is the heat transfer coefficient between mine water and the water flows through rocks, h_f^S is the salt transfer coefficient, R is the top (i.e., $z = 0$) temperature of rocks, the top temperature of the water flows through rocks, or the top salinity of the water flows through rocks on the two lateral boundaries, $r(z)$ is the linear function of either temperature (i.e., $r^T(z)$) or salinity (i.e., $r^S(z)$) in terms of depth z, and G is either the geothermal gradient or geochemical gradient. For Hancock Shaft 2, the parameters considering the above boundary conditions with Eq. (8) were set up as follows.

The top temperatures of rocks and the water flows through rocks of one lateral boundary (e.g., left) have the same value of 282.15 K, while the top temperature of the water flows through rocks of the other boundary (e.g., right) is 282.65 K, leading to a 0.5 K temperature difference to consider ΔF_f^T. The top salinity of the water flows through rocks of one lateral boundary, which has the top temperature of 282.15 K, is 0.01% and the top salinity on the other boundary is 0.06%, resulting in a 0.05% salinity difference to consider F_f^S. Rocks and the water flows through rocks have the same geothermal gradient of 5.35×10^{-3} K/m as that of mine water. The water flows through rocks have the same geochemical gradient of 5.18×10^{-4} \% /m as that of mine water when $N = 1.26$. h_{rf} was assumed to be 1 W/(m^2 K) due to the low velocity of mine water caused by the natural thermal convection according to [43]; while $h_f^T = 50$ W/(m^2 K) and $h_f^S = 10^{-4}$ m/(s \%) were assumed, for which heat convection between mine water and the water flows through rocks was not considered directly as illustrated above and this high value of h_f^T thus was used to indirectly consider such convection. It is noted that there has a vertical heat flux from deep bottom rocks to influence the temperature of mine water at the bottom surface. However, the bottom surface area in contact with the bottom rocks is much smaller than that of the surrounding rocks. Also, the value of h_{rf} is small. Therefore, this vertical heat flux was assumed to be negligible.

It is also significant to properly determine the effective kinematic viscosity and effective diffusivities. For large bodies of mine water in this study, we did not consider a turbulence model directly. Instead, the effective kinematic viscosity and effective diffusivities were assumed to be constant following a similar treatment in the numerical modeling of large-scale water circulations in oceans, e.g., Radko et al. [28]. For both effective thermal and solutal diffusivities, the effective diffusivity is the sum of the eddy diffusivity and the laminar diffusivity. For the thermal eddy diffusivity α_T, Eq. (9) can be used to estimate its magnitude [45]

$$\overline{\mathbf{U}'T'} = -\alpha_T \nabla T \tag{9}$$

where $\overline{\mathbf{U}'T'}$ is the eddy flux. According to Wolkersdorfer [27], the maximum velocity of mine water measured from tracer tests is in a magnitude of 10^{-2} m/s. α_T thus can be estimated under this velocity magnitude. Similarly, the solutal eddy diffusivity can be estimated by replacing T in Eq. (9) with S. The effective kinematic viscosity is also the sum of the eddy kinematic viscosity and the laminar kinematic viscosity. The eddy kinematic viscosity can be calculated based on the eddy thermal diffusivity and the turbulent Prandtl number. All the material properties of mine water used in this study are tabulated in Table 1. Field measurements for chemical concentrations [29] showed

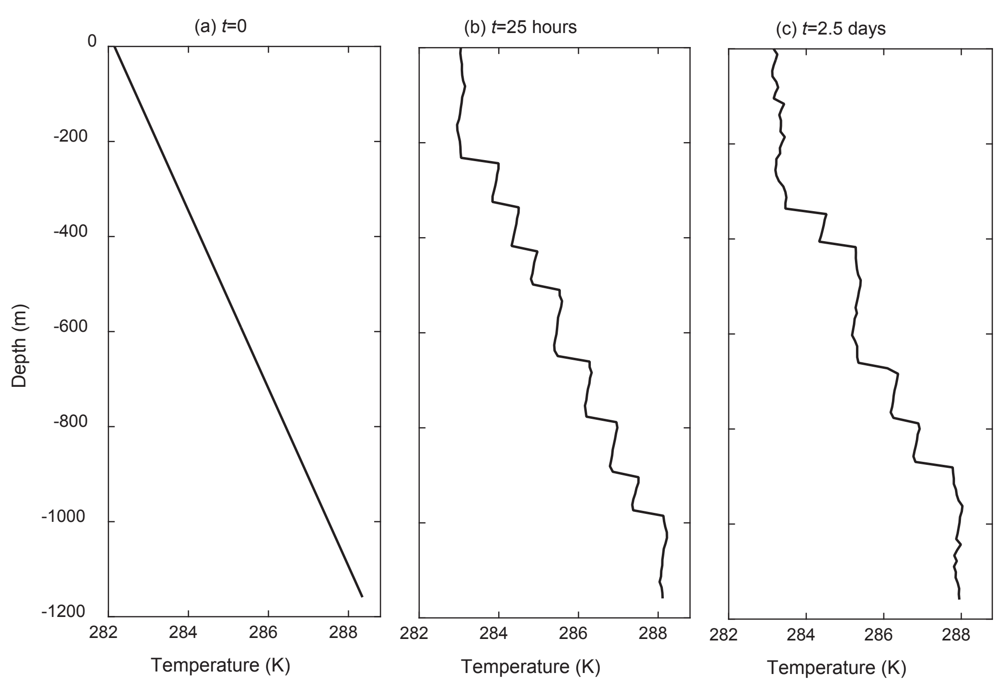

Fig. 9. Formation and evolution of stratifications for temperature when $N = 1.26$: (a) $t = 0$, (b) $t = 25$ h and (c) $t = 2.5$ days.

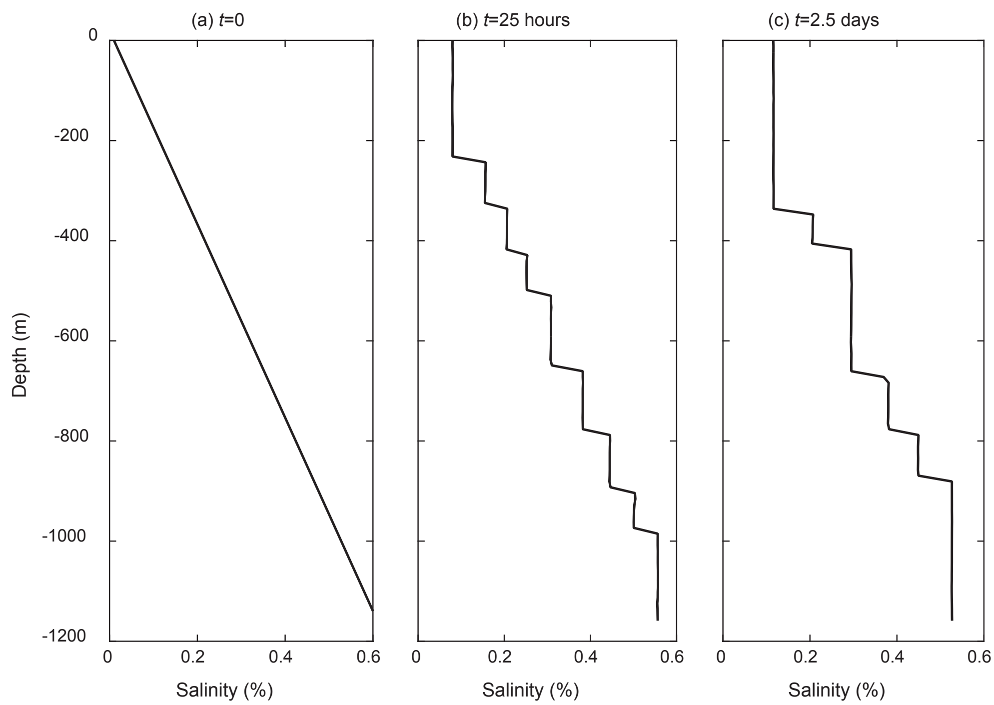

Fig. 10. Formation and evolution of stratifications for salinity when $N = 1.26$: (a) $t = 0$, (b) $t = 25$ h and (c) $t = 2.5$ days.

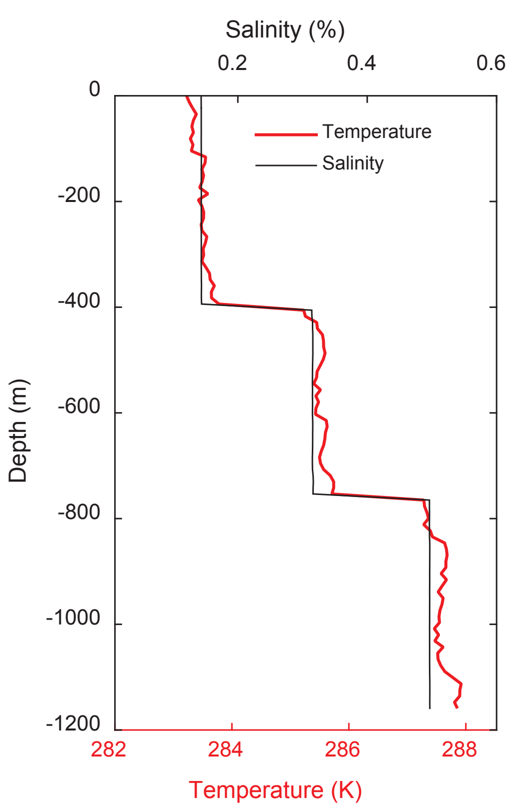

Fig. 11. Vertical distributions of temperature and salinity along the center axis of Shaft 2 when $N = 1.26$ at $t = 4.5$ days.

that sodium chloride is the primary chemical component in mine water. We, therefore, assumed the salinity in mine water represented by sodium chloride only for simplicity.

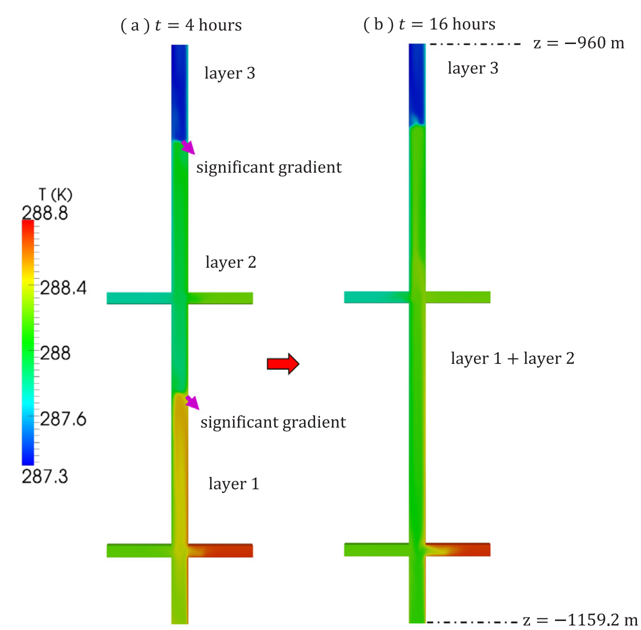

Fig. 12. Temperature contours in the elevation region between $z = -960$ m and $z = -1159.2$ m: (a) $t = 4$ h and (b) $t = 16$ h.

3. Results and discussion

3.1. Thermohaline stratification formation and evolution

In this section, multiphysics simulation with non-isothermal and non-isosolutal hydrodynamics is conducted using the validated model detailed in Section 2.2. This multiphysics simulation uses the material properties and the initial and boundary conditions introduced in Section 2.4 to predict the formation and evolution of thermohaline stratifications in mine water in Hancock Shaft 2.

Shown in Fig. 5 is the vertical distributions of temperature and salinity along the center axis of Shaft 2 when $N = 4$ at $t = 4.5$ days. It is

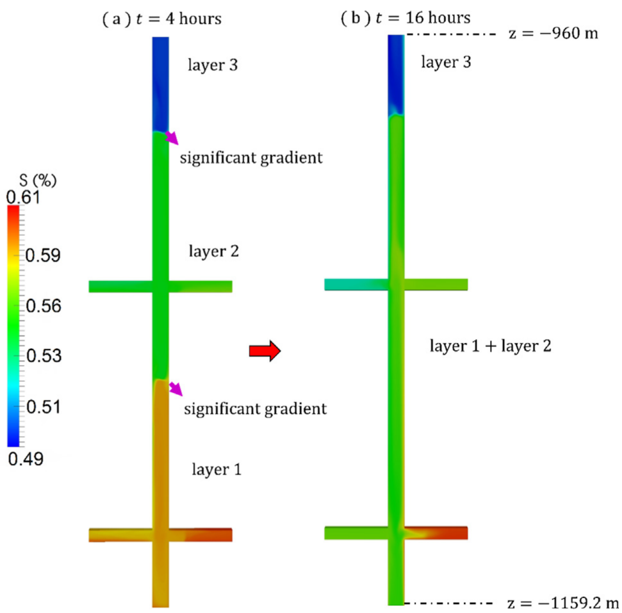

Fig. 13. Salinity contours in the elevation region between $z = -960$ m and $z = -1159.2$ m: (a) $t = 4$ h and (b) $t = 16$ h.

seen that thermohaline stratifications spontaneously occur and a "staircase" shape is exhibited. Each staircase represents an individual layer that has almost the same temperature and salinity. There are significant temperature and salinity gradients between two adjacent layers. The number of layers and the depth to form layers are highly identical for both temperature and salinity. This indicates that the double-diffusive intrusion caused by the lateral temperature and salinity fluxes can lead to thermohaline stratifications in large bodies of mine water.

The predicted velocity of mine water in the simulation also coincides with that of field measurements. Fig. 6 presents the variations of mine water velocity with respect to time in the center axis at $z = -470$ m. The maximum velocity is around 1 cm/s, which is highly consistent with the maximum magnitude of mine water velocity (i.e., 0.01 m/s) from field tracer tests [27]. As can be seen in Fig. 6, mine water velocity varies significantly before 15 h, while the variation of mine water velocity tends to be less significant after 15 h. This is because, initially, both temperature and salinity in mine water vary considerably due to the lateral double-diffusive intrusion, leading to the significant water movement with high velocities. As time elapses, relatively stable layers form so that mine water orderly circulates in each layer with relatively low velocities.

To clearly illustrate the formation of thermohaline stratifications, Fig. 7 shows the evolution of stratifications for salinity in the elevation region between $z = -360$ m and $z = -579.6$ m at different times. At $t = 7$ h, layers with different thicknesses are observed (Fig. 7a). As time elapses from 7 h to 25 h, the number of layers decreases. These observations in Fig. 7 indicate that layers merge gradually. Some of the small layers merge to form layers with a larger thickness, leading to a decrease in the number of layers. This phenomenon is similar to the layer-merging event in oceans obtained in the simulation with the gamma instability [28] introduced in Section 2.3.

The flow patterns in the same region can help illustrate variations of heat and mass in mine water, which trigger the formation and evolution of stratifications. As shown in Fig. 8, mine water is not stagnant and moves due to temperature and salinity differences. Mine water circulates to form separate layers (Fig. 8a). The water moves relatively fast within individual layers in the clockwise direction; while the velocity is very slow at the layer interfaces (Fig. 8b). As time elapses from $t = 25$ h to $t = 2.5$ days, the layer-merging happens and layers 1 and 2 merge to form one layer with a larger thickness. These observations of flow patterns in Fig. 8 clearly explain the layer-merging event for the salinity distributions and variations in Fig. 7.

Thermohaline stratifications can also be successfully reproduced with a small value of the buoyancy ratio N. Fig. 9 shows the evolution of stratifications for temperature along the center axis of Shaft 2 when $N = 1.26$. For calculating this N value, ΔT remains unchanged while ΔS decreases to be 0.6%. As shown in Fig. 9a, the initial temperature is linearly distributed. As time elapses, the smooth temperature distribution evolves to layers with significant temperature differences between layers (Fig. 9b and c). The layer-merging events also happen to form layers with a larger thickness by merging small layers. This interesting phenomenon can also be observed in Fig. 10 for salinity. The distribution of salinity evolves from the smooth linear distribution to layers with the stratified distribution, and then some of the layers merge into larger ones. As time further elapses, the thermohaline stratification presented in Fig. 11 has the same structure as the field

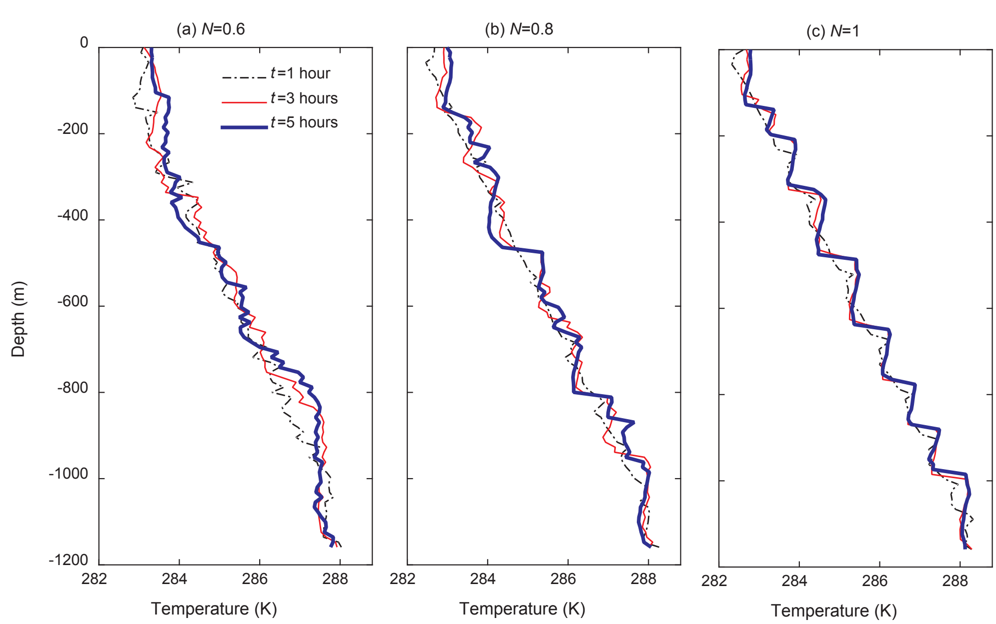

Fig. 14. Evolution of stratifications for temperature at different times with different N values: (a) $N = 0.6$, (b) $N = 0.8$ and (c) $N = 1$.

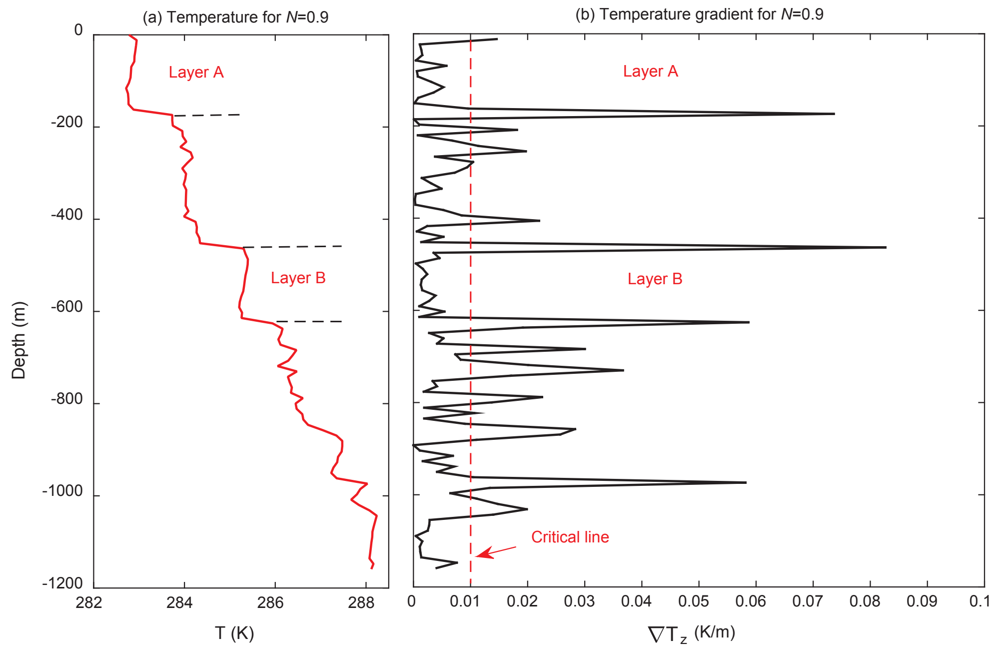

Fig. 15. Distributions of temperature along the center axis of Shaft 2 for $N = 0.9$ at $t = 5$ h: (a) temperature distribution and (b) absolute vertical temperature gradient.

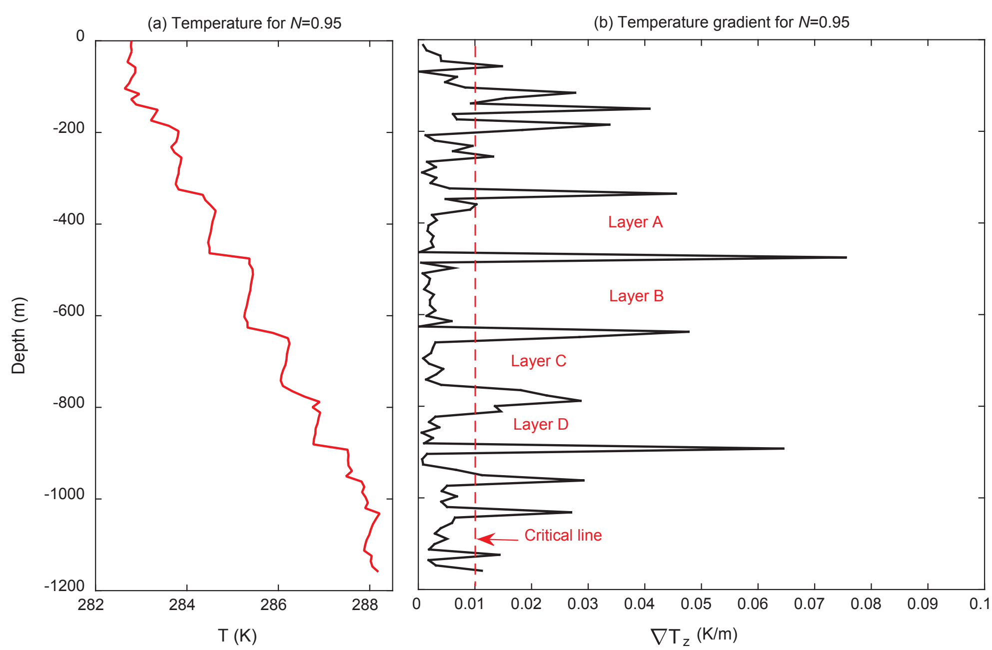

Fig. 16. Distributions of temperature along the center axis of Shaft 2 for $N = 0.95$ at $t = 5$ h: (a) temperature distribution and (b) absolute vertical temperature gradient.

observations in Fig. 1 with a few (2 or 3) layers.

Typical temperature and salinity contours are another way to directly show the heat and mass distribution within mine water. As shown in Fig. 12a, the temperature of each layer is almost the same. A significant temperature change exists between any two layers, which is consistent with stratifications in Figs. 9 and 10. At $t = 16$ h, layers 1 and 2 merge to form one layer that has the uniform temperature but a larger thickness (Fig. 12b). Similar observations also can be obtained in Fig. 13 for salinity contours. A clearly significant salinity gradient is observed between layers (Fig. 13a). Then, one large layer forms via merging layers1 and 2 when $t = 16$ h, as shown in Fig. 13b. These observations clearly show the formation and evolution of stratifications and layer-merging events in large bodies of mine water.

Observations presented in Figs. 5–13 clearly reveal the key heat and mass transport mechanisms for the formation and evolution of thermohaline stratifications. Dynamic DDC with the lateral double-diffusive intrusion (i.e., heat and salt fluxes) essentially triggers mine water movement to form layers of temperature and salinity from the smooth linear distributions. In each layer, the temperature and salinity will approach a constant value, making all the water appear as several layers with significant gradients. Then, some of the layers merge to form layers gradually with a larger thickness. The mechanisms inferred from the above observations well explain thermohaline stratifications in large bodies of mine water in field observations (see Fig. 1).

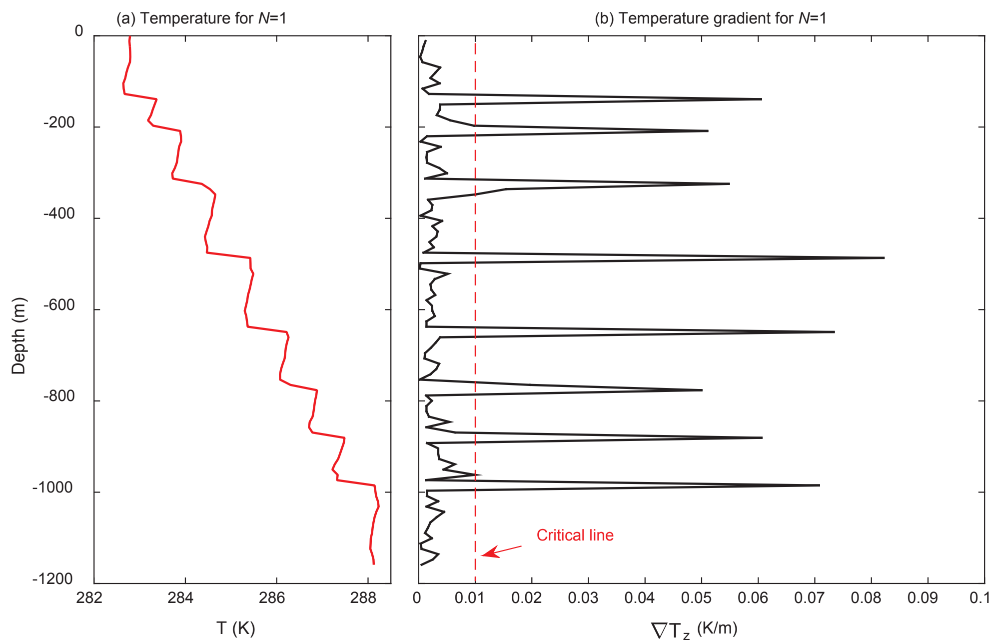

Fig. 17. Distributions of temperature along the center axis of Shaft 2 for $N = 1$ at $t = 5$ h: (a) temperature distribution and (b) absolute vertical temperature gradient.

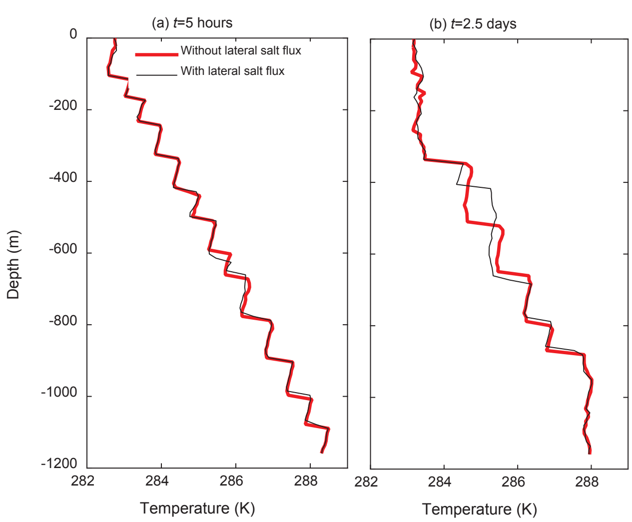

Fig. 18. Comparisons of temperature layers with and without the lateral salinity flux F_f^S: (a) $t = 5$ h and (b) $t = 2.5$ days.

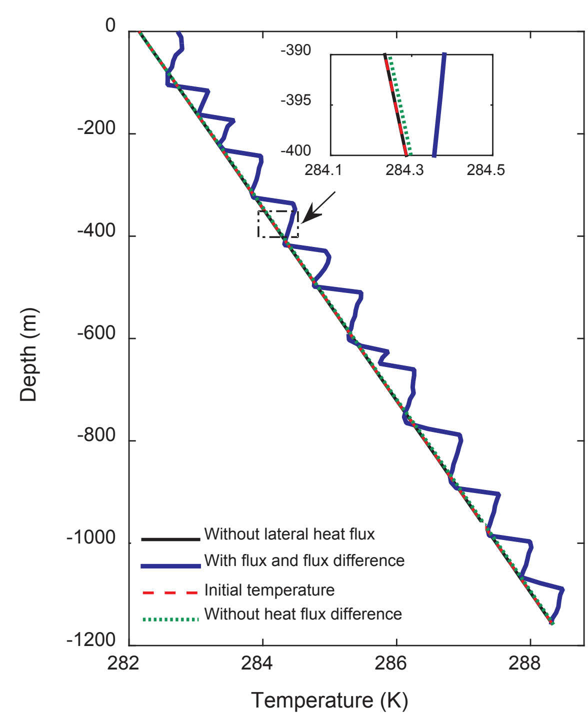

Fig. 19. Comparisons of the temperature distribution with and without the lateral heat flux F_f^T at $t = 5$ h.

For real heat extraction, one key consideration to determine the efficiency of heat pumps for extracting heat is the mine water temperature available to the pumps, which is determined by the temperature distribution in mine water and the pumping location. In addition, the variation of the temperature distribution (i.e., layered water structure) that is affected by the pumping rate and location and the natural energy and mass transport will further determine the future water temperatures available to the heat pumps. This will determine both the efficiency and sustainability of the whole geothermal application.

To be more specific, the thermohaline stratification can interact with the pumping location selection in a very complicated way. It is well known that the efficiency of heat pumps for heating can be enhanced by adopting a high water temperature. Therefore, the selection of the pumping location in the middle layer in Fig. 11 is better than that in the top layer. The use of such a deep pumping location in the middle layer, however, will make the pumping cost exceed the economic gain from the geothermal innovation, because the depth of the pumping location exceeds the economic limit depth of 305 m for pumping water according to a real application [41]. In fact, it is unnecessary to reach the middle or bottom layer to obtain a high water temperature. This is because, though slowly, the layers naturally merge; and consequently, the warm water in the middle or bottom layers will eventually move up to heat the relatively cold water in the top layer. Due to this reason, the water temperature in the top layer will increase naturally, even without heat extraction. Also, if the pumping location is in the top layer, heat extraction will reduce the water temperature in this layer. This essentially increases the temperature difference between the top and middle layers (i.e., N between the two layers decreases), as a result, further

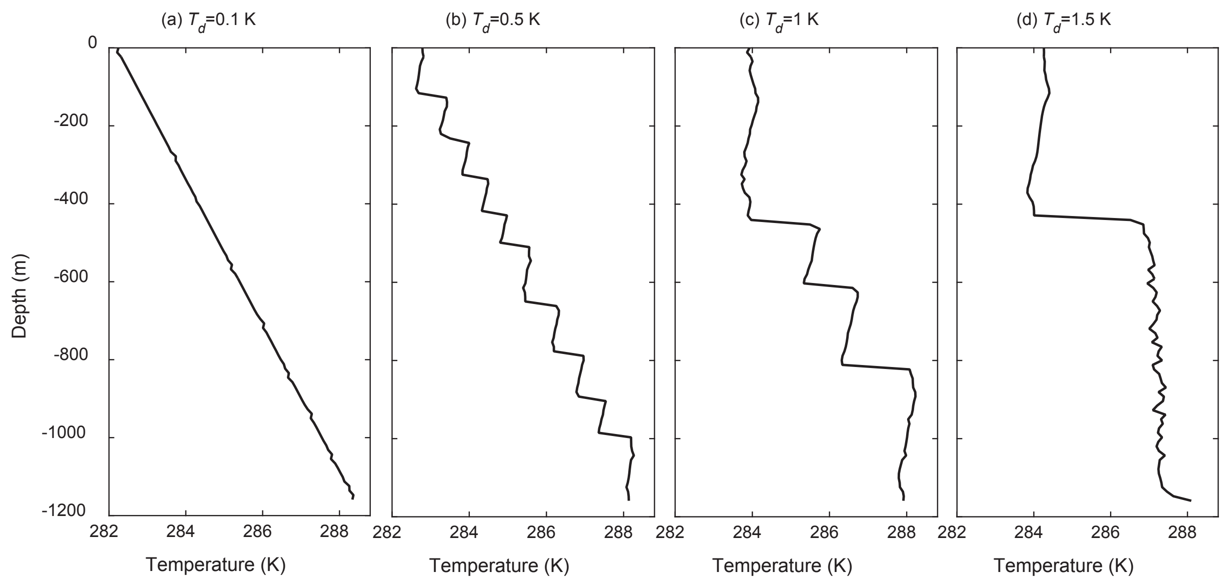

Fig. 20. Comparisons of temperature layers under different ΔF_f^T at t = 11 h and the corresponding temperature difference T_d is (a) 0.1 K, (b) 0.5 K, (c) 1 K, and (d) 1.5 K.

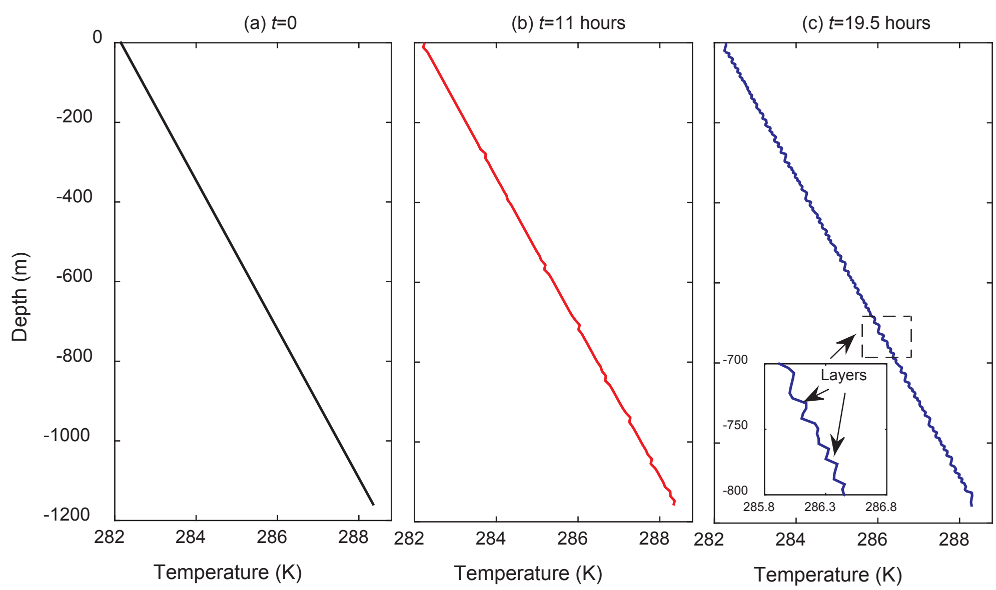

Fig. 21. Comparisons of the temperature distribution under the temperature difference T_d = 0.1 K at different times.

speeds up the layer-merging process.

In addition, the pumping rate will in return affect the layer-merging. This is because a pumping velocity is usually much higher than the natural mine water velocity. This high pumping velocity will significantly force the water movement to mix water with different temperatures and expedite the layer-merging. One possible scenario is that a high pumping rate could break the thermohaline stratification. As a result, the water temperature at the pumping location increases because the low-temperature water in the top layer mixes with the high-temperature water from lower layers. This is, however, beyond the scope of this study and further studies are needed to confirm the possibility and discuss the potential implications of such events on the efficiency and sustainability of the geothermal application with mine water.

3.2. Critical buoyancy ratio for thermohaline stratification

In oceans, no salt-finger staircases have been observed when the critical buoyancy ratio N_c is smaller than 0.5 and N_c needs to be larger than 0.59 to obtain thermohaline staircases [28]. In this section, we explore the critical buoyancy ratio N_c for the formation of thermohaline stratifications in large bodies of mine water. As the temperature layers are highly identical to the salinity layers in thermohaline stratifications (see Fig. 11), we only focus on the evolution of the temperature distribution in this section.

Fig. 14 presents the evolution of the temperature distribution along the center axis of Shaft 2 when N differs. As shown in Fig. 14a, temperature layers cannot be observed during the first 5 h when N = 0.6. This N value is almost the same as the critical buoyancy ratio of 0.59 for thermohaline staircases in oceans. The results in Fig. 14a imply that such a low value of N fails to provide enough salinity difference-induced buoyancy force to suppress the thermal convection. Therefore, the thermal convection is significant in the whole dynamic DDC process when N = 0.6. As N increases to 0.8, as shown in Fig. 15b, a few layers may form in local regions, but they are very obscure. Clear layers are observed at the same calculation time when N = 1, as shown in Fig. 15c. The preliminary observations in Fig. 15 reveal that N_c for the formation of clear layers in mine water is greater than 0.8 but smaller or equal to 1.0.

In order to accurately obtain N_c for thermohaline stratifications in mine water, $N = 0.9$, $N = 0.95$, and $N = 1$ were investigated. Fig. 15a shows the temperature distribution for $N = 0.9$ at $t = 5$ h. Two clear temperature layers, i.e., Layer A and Layer B, can be observed. The absolute vertical temperature gradient for the same N is shown in Fig. 15b. It is seen that the vertical temperature gradient is very close and smaller than 0.01 K/m within Layer A and Layer B. This is because if a temperature layer forms, the temperature in each layer is almost the same, leading to a very small vertical temperature gradient within each layer. Based on this, 0.01 K/m was adopted as the critical value for a criterion for the layer determination. In this criterion, a temperature layer forms if the vertical temperature gradient is smaller than 0.01 K/m within a vertical depth range (i.e., a temperature layer). No layers form beyond 0.01 K/m.

For $N = 0.95$ at $t = 5$ h, four temperature layers, i.e., Layers A-D, can be easily identified based on the criterion (see Fig. 16b). The number of layers increases when N increases from 0.9 to 0.95. As shown in Fig. 17b, nine layers can be clearly determined in the whole region at the same calculation time when N increases to 1.0. The results from Figs. 15–17 indicate that obscure layers can still be observed at the same calculation time when the value of N is equal to 0.95. Once N is equal to 1.0, clear layers can be observed in the whole region. Therefore, the critical buoyancy ratio N_c is suggested to be 1.0 for producing layers in mine water with a clear structure that is very similar to field observations in Fig. 1.

3.3. Is the lateral double-diffusive intrusion required for thermohaline stratifications?

According to the first hypothesis [37] introduced in Section 2.3, the major cause for the formation of thermohaline staircases in oceans is the double-diffusive intrusion due to lateral temperature and salinity fluxes. As for large bodies of mine water, this hypothesis has been proven by the transient simulation detailed in Section 3.1. The intrusion due to the lateral salinity flux is common in oceans due to the salt transport by water circulations. It is also possible in some mines flooded by salty underground water, e.g., abandoned mines in southwestern Indiana in the U.S. [46]. However, the lateral salinity flux is possibly negligible to water in some mines, where the salinity of mine water is the same as fresh groundwater or surface water, e.g., flooded mines in the U.P. of Michigan. Therefore, this raises an interesting question: "Are the lateral temperature and salinity fluxes required for the formation of thermohaline stratifications in large bodies of mine water?" Such a question will be answered in this section with $N = 1.26$.

The lateral salinity flux is investigated first. For the purpose, no salinity flux was applied to the lateral boundaries. The temperature distributions in Fig. 18 reveal that thermohaline stratifications can still form without the lateral salinity flux. By comparing the temperature layers with and without the lateral salinity flux, we found that the only difference is the different layer numbers. The reason is that considering the lateral salinity flux will increase the salinity in the mine water environment, which essentially increases the buoyancy ratio N, as a result, suppressing the thermal convection for merging layers. Therefore, the layer-merging process caused by the thermal convection becomes slow and the layer number with the lateral salinity flux is larger than that without such a flux. Therefore, the lateral salinity flux is not required for the formation of thermohaline stratifications. In fact, the lateral salinity flux considered in the above simulation in Section 3.1 (e.g., Figs. 7, 9 and 10) is negligible. This is because the mass transfer coefficient (i.e., $h_f^S = 10^{-4}$ m/(s \%)) is very small. Accordingly, the amount of salinity intruded into the mine water environment via the lateral salinity flux F_f^S calculated with Eq. (8) is very small.

To investigate whether the lateral heat flux (i.e., F_f^T) from the water flows through rocks is required or not, the heat flux was not applied to the lateral boundaries. Comparisons of temperature distributions with and without the lateral heat flux in Fig. 19 reveal that the lateral heat flux F_f^T is a required condition. In addition to that, a difference between the lateral heat fluxes (i.e., ΔF_f^T in Fig. 4a) is also required. As shown in Fig. 19, the temperature distribution without the lateral heat flux is linear and almost the same as the original distribution. A similar observation can be obtained for the situation without ΔF_f^T. Temperature layers can only be observed if ΔF_f^T is considered.

Since the formation of thermohaline stratifications requires the lateral heat flux with ΔF_f^T, it is helpful to understand how ΔF_f^T influences the formation and evolution of thermohaline stratifications. For this purpose, the value of ΔF_f^T varies, which can be calculated using the temperature difference T_d between the lateral boundaries using the below equation

$$\begin{cases} \Delta F_f^T = h_f^T(r^{T,1}(z) - r^{T,2}(z)) \\ \quad T_d = r^{T,1}(z) - r^{T,2}(z) \end{cases} \tag{10}$$

where $r^{T,1}(z)$ is the linear temperature function with depths for the one lateral boundary and $r^{T,2}(z)$ is the linear temperature function with depths for the other lateral boundary. As introduced in Section 2.4, the water flows through rocks have the same geothermal gradient of 5.35×10^{-3} K/m. Therefore, $T_d = r^{T,1}(z) - r^{T,2}(z)$ can be obtained, which is a constant and independent of depth z.

The influence of ΔF_f^T on thermohaline stratifications is significant, as shown in Fig. 20. At the same calculation time, the higher the value of ΔF_f^T, which is calculated with a higher T_d, the smaller the number of layers. This is because a higher ΔF_f^T will increase the temperature in the mine water environment, which decreases the buoyancy ratio N, consequently, expediting the thermal convection for merging layers. Therefore, the layer number becomes smaller with an increase in ΔF_f^T. It is also seen in Fig. 20a that no layers form under$T_d = 0.1$ K, when ΔF_f^T is very small. However, as shown in Fig. 21, layers can be clearly observed when time elapses from 11 h to 19.5 h, though the layers are very small. This indicates that the formation and evolution of thermohaline stratifications under a small ΔF_f^T is very slow.

The above simulation results in this section reveal that two conditions are required to reproduce thermohaline stratifications in large bodies of mine water: (1) the lateral heat flux and (2) a difference between the lateral heat fluxes (i.e., ΔF_f^T). The value of ΔF_f^T determines the speed for the formation and evolution of thermohaline stratifications. At the same calculation time, the smaller the value of ΔF_f^T, the greater the layer number.

4. Conclusions

No scientific explanation is available for the layering phenomenon of both temperature and salinity in large bodies of subterranean water (e.g., mine water), i.e., thermohaline stratification, which is commonly observed in mine water. Such a phenomenon, however, is very significant to the application of geothermal energy recovery from flooded mines by determining the temperature distribution and consequently the reserve and efficiency of the energy resource. This study addresses this key scientific issue by predicting the formation and evolution of thermohaline stratifications in large bodies of mine water via multiphysics simulation with unique non-isothermal and non-isosolutal hydrodynamics.

The simulation, for the first time, succeeded in explaining the key heat and mass transport mechanisms in the dynamic double-diffusive convection process and reproducing the layering phenomenon in large bodies of mine water. The simulation results proved that the double-diffusive intrusion caused by lateral temperature and salinity fluxes can lead to thermohaline stratifications in the large-scale mine water with initially linear distributions of temperature and salinity. In the evolution of thermohaline stratifications, the layer-merging event is involved. Some of the small layers gradually merge to form layers with a larger thickness, leading to a decrease in the number of layers.

The simulation results also revealed that the buoyancy ratio is a key parameter for producing clear thermohaline stratifications in the large-scale mine water and its critical value was suggested to be 1.0 based on the proposed criterion for the layer determination. To successfully reproduce thermohaline stratifications in large bodies of mine water, the lateral salinity flux was found to be a not required condition. The required condition is the lateral heat flux. In addition, a difference between lateral heat fluxes is also required. Thermohaline stratifications can be observed as long as the lateral heat flux with a difference between the lateral heat fluxes is considered.

No research has been reported prior to the current study for scientifically explaining the formation and evolution of thermohaline stratifications. It is the first time, to the best of our knowledge, that thermohaline stratifications in large-scale subterranean water bodies have been successfully reproduced. This will provide a solid scientific basis for the geothermal application using subterranean water. It is believed that this scientific breakthrough is significant for the future design of recovering geothermal energy from flooded mines (e.g., target temperature layers and mine water pumping locations) considering thermohaline stratifications in an efficient, sustainable, and economical way.

References

[1] Rybach L. Geothermal energy: sustainability and the environment. Geothermics 2003;32:463–70.
[2] Lund JW, Freeston DH, Boyd TL. Direct application of geothermal energy: 2005 worldwide review. Geothermics 2005;34:691–727.
[3] Rybach L, Mongillo M. Geothermal sustainability – a review with identified research needs. GRC Trans 2006;30:1083–90.
[4] Milora SL, Tester JW. Geothermal energy as a source of electric power. Geol Mag 1977;114:1–3.
[5] Bertani R. Geothermal power generation in the world 2005–2010 update report. Geothermics. 2012;41:1–29.
[6] Ochsner K. Geothermal heat pumps: a guide for planning and installing. New York, NY, USA: Routledge; 2012.
[7] Self SJ, Reddy BV, Rosen MA. Geothermal heat pump systems: status review and comparison with other heating options. Appl Energy 2013;101:341–8.
[8] Chua KJ, Chou SK, Yang W. Advances in heat pump systems: a review. Appl Energy 2010;87:3611–24.
[9] Ramos EP, Breede K, Falcone G. Geothermal heat recovery from abandoned mines: a systematic review of projects implemented worldwide and a methodology for screening new projects. Environ Earth Sci 2015;73:6783–95.
[10] Jessop A. Geothermal energy from old mines at Springhill, Nova Scotia, Canada. Nova Scotia, Canada; 1995. p. 463–8.
[11] Allen D, Ghomshei M, Sadler-Brown T, Dakin A, Holtz D. The current status of geothermal exploration and development in Canada. Proceedings from world geothermal congress, Japan. 2000:55–8.
[12] Malolepszy Z. Low temperature, man-made geothermal reservoirs in abandoned workings of underground mines. USA: Stanford University; 2003. p. 259–65.
[13] Bazargan B, Demollin E, Van Bergermeer J-J. Geothermal use of deep flooded mines. Proc of the post mining symposium. Nancy, France; 2008. p. 1–10.
[14] Wieber G, Pohl S. Mine water: a source of geothermal energy-examples from the Rhenish Massif. In: 10th International mine water association congress: mine water and the environment. Ostrava, Czech Republic: Technical University of Ostrava; 2008. p. 1–4.
[15] Loredo J, Ordóñez A, Jardón S, Álvarez R. Mine water as geothermal resource in Asturian coal mining basins (NW Spain). Proceedings of 11th international mine water association congress. Aachen, Germany; 2011. p. 177–82.
[16] Raymond J, Therrien R, Hassani F. Overview of geothermal energy resources in Québec (Canada) mining environments. 10th International mine water association congress: mine water and the environment. Ostrava, Czech Republic: Technical University of Ostrava; 2008. p. 1–12.
[17] Hall A, Scott JA, Shang H. Geothermal energy recovery from underground mines. Renew Sustain Energy Rev 2011;15:916–24.
[18] Hasche-Berger A. Hydrodynamics in a flooded underground limestone mine. Reliable mine water technology. USA: Golden CO; 2013. p. 1165–72.
[19] Preene M, Younger P. Can you take the heat? – Geothermal energy in mining. Min Technol 2014;123:107–18.
[20] Al-Habaibeh A, Athresh AP, Parker K. Performance analysis of using mine water from an abandoned coal mine for heating of buildings using an open loop based single shaft GSHP system. Appl Energy 2018;211:393–402.
[21] Athresh AP, Al-Habaibeh A, Parker K. The design and evaluation of an open loop ground source heat pump operating in an ochre-rich coal mine water environment. Int J Coal Geol 2016;164:69–76.
[22] Raymond J, Therrien R. Optimizing the design of a geothermal district heating and cooling system located at a flooded mine in Canada. Hydrogeol J 2014;22:217–31.
[23] Raymond J, Therrien R. Low-temperature geothermal potential of the flooded Gaspé Mines, Québec, Canada. Geothermics 2008;37:189–210.
[24] Streb C, Wieber G. Geothermal energy from a flooded mine: a hydraulic model. In: Rüde RT, Freund A, Wolkersdorfer Ch., editors. Mine water-managing the challenges. IMWA; 2011. p. 189–93.
[25] Arias CA, Alonso AO, García RÁ. Hydrogeological and thermal modelling of an underground mining reservoir. Mathematics of planet earth. Springer; 2014. p. 419–23.
[26] Bao T, Liu Z. Large-scale thermo-hydrodynamic modeling of a flooded underground mine for geothermal applications. Geo-Chicago 2016: ASCE 2016:72–83.
[27] Wolkersdorfer C. Water management at abandoned flooded underground mines: fundamentals, tracer tests, modelling, water treatment. München, Germany: Springer Science & Business Media; 2008.
[28] Radko T, Bulters A, Flanagan J, Campin J-M. Double-diffusive recipes. Part I: Large-scale dynamics of thermohaline staircases. J Phys Oceanogr 2014;44:1269–84.
[29] Bao T, Liu Z, Meldrum J, Green C, Xue P, Vitton S. Field tests and multiphysics analysis of a flooded shaft for geothermal applications with mine water. Energy Convers Manage 2018;169:174–85.
[30] Hamm V, Sabet BB. Modelling of fluid flow and heat transfer to assess the geothermal potential of a flooded coal mine in Lorraine, France. Geothermics 2010;39:177–86.
[31] Turner J. Double-diffusive phenomena. Annu Rev Fluid Mech 1974;6:37–54.
[32] Reichart G, Vaute L, Collon-Drouaillet P, Buès MA. Modelling heat and salinity related convective processes in deep mining flooded wells. In: 11th International mine water association congress. Aachen, Germany; 2011. p. 183–7.
[33] Ferziger JH, Peric M. Computational methods for fluid dynamics. Springer Science & Business Media; 2012.
[34] Oliveira PJ, Issa RI. An improved PISO algorithm for the computation of buoyancy-driven flows. Numer Heat Transf: Part B: Fund 2001;40:473–93.
[35] Lee J, Hyun M, Kang Y. Confined natural convection due to lateral heating in a stably stratified solution. Int J Heat Mass Transf 1990;33:869–75.
[36] Lee JW, Hyun JM. Double diffusive convection in a cavity under a vertical solutal gradient and a horizontal temperature gradient. Int J Heat Mass Transf 1991;34:2423–7.
[37] Merryfield WJ. Origin of thermohaline staircases. J Phys Oceanogr 2000;30:1046–68.
[38] Kelley D, Fernando H, Gargett A, Tanny J, Özsoy E. The diffusive regime of double-diffusive convection. Prog Oceanogr 2003;56:461–81.
[39] Radko T. A mechanism for layer formation in a double-diffusive fluid. J Fluid Mech 2003;497:365–80.
[40] Butler BS, Burbank WS. The copper deposits of Michigan. US Government Printing Office; 1929.
[41] Liu Z, Meldrum J, Xue P, Green C. Preliminary studies of the use of abandoned mine water for geothermal applications. IFCEE 2015;2015:1678–90.
[42] Apple BA, Reeves HW. Summary of hydrogeologic conditions by county for the state of Michigan. Reston, Virginia, USA: Geological Survey (US); 2007.
[43] Zhao Z. On the heat transfer coefficient between rock fracture walls and flowing fluid. Comput Geotech 2014;59:105–11.
[44] Hull JR, Nielsen J, Golding P. Salinity gradient solar ponds. Boca Raton, FL (USA): CRC Press Inc.; 1988.
[45] Vallis GK. Atmospheric and oceanic fluid dynamics. Cambridge University Press; 2017.
[46] Bayless ER, Olyphant GA. Acid-generating salts and their relationship to the chemistry of groundwater and storm runoff at an abandoned mine site in southwestern Indiana, USA. J Contam Hydrol 1993;12:313–28.